Advanced Wood Damage Detection and Monitoring Using Instantaneous Frequency Analysis of Acoustic Emission Signals

Xinci Li
Minghua Wang
Ming Li
Chuanzhi Fang

Abstract

In order to obtain the acoustic emission (AE) signals of hardwood and softwood in the process of bending failure, and to evaluate their damage degree, this article proposes a method to identify AE events based on the instantaneous frequency of the AE signal and dynamic monitoring of the wood damage based on the density statistics of AE events. First, air-dried *Zelkova schneideriana* and *Pinus sylvestris* var. *mongolica* samples were used for the bending test, and the original AE signal was collected using a three-channel NI USB-6366 high-speed data acquisition card. Second, a wavelet transform was used to reduce the noise of the original AE signal, and then the deformation AE, microfracture AE, and fracture AE events were defined according to the frequency domain distribution and causes of the AE signal and the damage images of the specimens. Finally, the Hilbert transform was used to obtain the instantaneous frequency of the AE signal, and then the occurrence densities of the three types of AE events were counted based on the instantaneous frequency. The density curves of AE events were then utilized to distinguish the damage characteristics of the two specimens, and to determine and predict the stress release and damage trends of wood under loading. The experimental results show that defining and counting AE events in the frequency domain based on the instantaneous frequency of the AE signal can better reflect the stress level of the material, so as to objectively evaluate and predict the degree and trend of wood damage.

Wooden materials have a wide range of applications in daily life. When they are used as stressed components, their strength, stress, strain, and other mechanical properties that will affect their safety should be monitored to facilitate the maintenance and practical application of wooden components. Acoustic emission (AE) refers to the elastic waves generated within a material when stored strain energy is suddenly released as a result of irreversible changes in its internal microstructure (Nasir et al. 2022). In the case of wood, different tree species affect the characteristics of the AE signals due to differences in their internal grain, porosity, health condition, and so on. In addition, the moisture content and temperature of wood also affect the generation and propagation of AE signals (Kang and Booker 2002, Chan et al. 2011). Li et al. (2023) found that the angle of incidence also affects the propagation law of the AE signal, and they changed the angle of incidence of the AE source by sawing out wood specimens with different angles. The energy attenuation rate of the AE signal decreases with increasing angle of incidence and is greatest when the AE signal is incident in the direction perpendicular to the grain of the wood, i.e., when the inclination angle is 0°.

Acoustic emission technology (AET), as an active nondestructive technique (Ding et al. 2015, Shen et al. 2015,

The authors are, respectively, Lecturer, School of Mechanical Engineering, Anhui Inst. of Information Technol., Wuhu, China (xcli18@126.com [corresponding author]); PhD Candidate, School of Aerospace Engineering, Xiamen Univ., Xiamen, China (wangmingh1218@163.com); PhD/Professor/Doctoral Supervisor, School of Machinery and Transportation Engineering, Southwest Forestry Univ., Kunming, China (swfu_lm@swfu.edu.cn); PhD/Associate Professor, School of Mechanical Engineering, Anhui Inst. of Information Technol., Wuhu, China (fangchuanz@163.com). This paper was received for publication in December 2024. Article no. 24-00056.

Forest Prod. J. 75(3):217–228.
doi:10.13073/FPJ-D-24-00056

Huang et al. 2018), is increasingly used in the study of the damage evolution of materials such as composites, magnetic materials, and metals, as it enables real-time dynamic nondestructive evaluation of the properties of AE sources based on the AE signals generated by the material under load (Sun et al. 2006a, 2006b). In the field of wood science, AET has been mainly used to monitor drying (Kowalski et al. 2004), detect defects (Ritschel et al. 2014), and study the fracture behavior of wood under load (Jakieła et al. 2008, Guo et al. 2019), and many more. Noguchi et al. (1985) counted the AE cumulative event count, the AE event count rate, and the amplitude distribution of the AE signal during the drying process of hardwood and softwood specimens, respectively, and analyzed the waveform and spectrum of the AE signal. Sadanari and Kitayama (1989) qualitatively investigated the relationship between AE characteristic parameters and drying conditions such as temperature and humidity, as well as surface cracking, using AE characteristic values such as ring counts, peaks, etc. Kowalski and Smoczkiewicz (2004) used AE energy curves to characterize the tendency of wood to shrink and crack during the drying process. For the delamination propagation behavior of boards under loading, Rescalvo et al. (2020) proposed a delamination prediction method for poplar boards based on the AE activity (localized event rate) and the AE intensity (signal strength). Mohammadi et al. (2015) investigated the layered evolutionary behavior of carbon/epoxy laminated composites under different load types using modified AET and characterized the crack length based on the cumulative AE energy. In studies of differences in material AE characteristics, it was found that older wood produced more AE events and experienced longer crack propagation before final fracture than new wood (Ando et al. 2006). Hardwood produced more AE counts before cracking than softwood under the same loading conditions, while softwood had higher AE counts after cracking than hardwood, and both woods had microcracks before visible cracks. In addition, hardwoods have more significant linear elastic properties in the fracture mode, while softwoods have more malleable fracture patterns (Chen et al. 2006b). In addition, in the related studies on the identification of wood fracture patterns, it was found that AE signals with high frequency and high amplitude were generated by fiber fracture. The high-frequency and low-amplitude signals originated from the evaporation of wood water, while the AE signals with low frequency and low amplitude were caused by matrix cracks or interfacial cracks (Choi et al. 2007, Shao et al. 2009). The characteristics of AE signals corresponding to cell-wall fracture were high amplitude, high energy, and long duration, while those corresponding to cell-wall interface injury and crushing injury were low amplitude, low energy, and short duration (Ding et al. 2012). Moreover, crack extension and aggregation produced higher amplitude and energy than crack sprouting (Wang et al. 2020). Zhao et al. (2020) developed a theoretical model for crack destabilization prediction by monitoring the AE activity and location of crack tips within wood. Li et al. (2020) found that moisture content affects the AE signals during wood damage, with air-dried wood producing the most AE signals and the most frequent abrupt changes in AE events during loading, while water-saturated wood had the fewest AE signals and the least damage. Wu et al. (2023) proposed a relationship between the damage mechanism of a glass fiber reinforced polymer-balsa composite sandwich under static four-point bending and the AE amplitude, peak frequency, and duration by AE monitoring and microscopic observation.

Most of the aforementioned studies analyzed the damage characteristics of materials through time-domain parameters such as AE events and AE energy. Because wood is a nonhomogeneous biocomposite material (Zhao et al. 2011), the AE signal has a stronger attenuation during propagation and is easily covered by noise. The AE signal is a nonstationary signal with strong randomness (Gong et al. 2013), and there is large uncertainty in the time-domain parameters, which creates a big challenge for the parametric analysis method based on the time-domain signal. Moreover, damage fracturing of wood is a multiscale, nonlinear kinetic process, and characterization of this type of damage using parametric analysis loses the waveform information that best reflects the AE damage characteristics of the material, and so parametric analysis can only qualitatively evaluate the damage of the material. The instantaneous frequency does not depend on the global information of the signal when characterizing the nonstationary signal, and it has unique instantaneous validity, fully reflecting the local characteristics of the signal and the nonlinear time-varying characteristics of the vibration response (Chen et al. 2006a, Yuan et al. 2016). Existing relevant studies have shown that defining and counting AE events based on instantaneous frequency provided a clearer physical meaning, which can objectively reflect the stress level and damage trend of material during the damage process (Fang et al. 2018, Dong and Li 2020, Ju et al. 2020, Li et al. 2020). Therefore, to address the problem of damage evaluation during bending loading of hardwoods and softwoods, this study used air-dried *Zelkova schneideriana* and *Pinus sylvestris* var. *mongolica* samples as test materials to conduct a three-point bending damage test and then defined different types of AE events in the frequency domain based on the characteristics of the AE signals generated when the material released strain energy. Then, statistical analysis of AE events was performed based on the instantaneous frequency of the AE signals, so as to identify and characterize the type and degree of damage of the wood in the frequency domain.

Materials and Methods

Experimental materials

In order to study the AE characteristics of different tree species under load, common hardwood (*Z. schneideriana*) and softwood (*P. sylvestris* var. *mongolica*) samples were selected as test materials and used to make specimens with dimensions of 800 by 60 by 30 mm (axial by tangential by radial), and the number of specimens for each species was two, numbered as ZS1, ZS2, PSM1, and PSM2, respectively. The density and absolute moisture content of the specimens of *Pinus sylvestris* var. *mongolica* and *Zelkova schneideriana* in the air-dry state were 0.458 g/cm^3 and 11.1 percent and 0.705 g/cm^3 and 14.3 percent, respectively.

The three-point bending tests for the test piece were carried out using a UTM5105 mechanical testing machine (Jinan Kason Testing Equipment Co., Ltd.) at a loading speed of 2 mm/min and a span of 200 mm. Based on the NI USB-6336 high-speed data acquisition card (National

Instruments) and LabVIEW software, a three-channel AE signal acquisition platform was built with a maximum sampling frequency of 2 MHz for each channel. The sensor was an SR-150N single resonant AE sensor (Beijing Soundwel Technology Co., Ltd.) with a bandwidth of 22 kHz to 220 kHz, and a power amplifier interface (PAI) front-end amplifier (Soundwel) with a gain of 40 dB was used to amplify the signal detected by the AE sensor for long-distance transmission of the AE signal. The study showed that the maximum frequency of the AE signal of the wood was about 200 kHz. According to the Shannon sampling theorem, in order to restore the analog signal without distortion, the sampling frequency f_s and the maximum frequency f_{max} of the signal must satisfy $f_s \geq 2 f_{max}$. Therefore, in the experimental process, the sampling frequency of each channel of the system was set to 500 kHz, and the output voltage range was set to (−5 V, 5 V).

Experimental methods

As shown in Figure 1, the sensors S_{AE1}, S_{AE2}, and S_{AE3} were equally spaced at 300-mm intervals on the upper surface of the specimen, in which the sensor S_{AE1} was placed 100 mm away from the left-end face of the specimen, and the load was applied in the middle position between sensor S_{AE1} and sensor S_{AE2} by the universal mechanical testing machine for three-point bending tests. In order to ensure sufficient coupling between the sensor and the specimen, high-temperature vacuum insulating grease was filled between the specimen and the sensor to reduce the influence of the air medium on the test results. In addition, the sensor was fixed on the surface of the specimen with a rubber band.

Due to the influence of environmental noise, the original signal collected was mixed with ambient random noise. The discrete wavelet transform method has excellent denoising effect and time–frequency localization analysis capability, which can realize signal denoising and reconstruct the AE signal waveform at the same time. The principle of wavelet denoising is to decompose the collected original AE signal into different frequency bands to obtain a series of low-frequency approximate signals and high-frequency detail signals and then filter out the noise according to the difference between the noise and the effective signal under the wavelet transform. This study used the Daubechies wavelet as the discrete wavelet transform basis function for the five-layer wavelet decomposition. In the original signal acquisition process, each channel sampling frequency $f_s = 500$ kHz. According to the Shannon sampling theorem, the AE signal analysis frequency $f_h = f_s/2 = 250$ kHz; that is, theoretically, the signal components can effectively be identified in the range of 0 to 250 kHz. According to the wavelet multi-resolution analysis principle, the frequency bands of each layer of high-frequency detail signals after wavelet decomposition were (125 kHz, 250 kHz), (62.5 kHz, 125 kHz), (31.25 kHz, 62.5 kHz), (15.625 kHz, 31.25 kHz), (7.8125 kHz, 15.625 kHz) . . . . This means that only five layers of decomposition were needed to cover the full measurement range of the SR-150N single resonant AE sensor.

In order to define AE events more objectively in the frequency domain and identify AE characteristics in the process of material damage, an empirical mode decomposition (EMD) algorithm was used to decompose the AE signal decomposed and reconstructed by the discrete wavelet transform into a series of intrinsic mode functions (IMFs). The IMF with the highest correlation with the reconstructed signal was used as the final AE signal, and the instantaneous frequency of this AE signal was obtained by the Hilbert transform. The basic process is shown in Figure 2.

For any continuous time signal $Y(t)$, its Hilbert transform $H[Y(t)]$ is:

$$H[Y(t)] = \frac{1}{\pi} P \int_{-\infty}^{+\infty} \frac{Y(\tau)}{t-\tau} d\tau \tag{1}$$

where P is the Cauchy principal value integral and τ is the time variable. Construction of an analytical signal $Z(t)$ from the real signal $Y(t)$ and its Hilbert transform $H[Y(t)]$ is done by:

$$Z(t) = Y(t) + iH[Y(t)] = a(t)e^{i\theta(t)} \tag{2}$$

where $a(t)$ is the instantaneous amplitude, and $\theta(t)$ is the phase:

$$a(t) = \sqrt{Y^2(t) + H^2[Y(t)]}$$

$$\theta(t) = \arctan\left(\frac{H[Y(t)]}{Y(t)}\right) \tag{3}$$

The instantaneous frequency is calculated as follows:

$$f(t) = \frac{1}{2\pi}\omega(t) = \frac{1}{2\pi} \times \frac{d\theta(t)}{dt} \tag{4}$$

The instantaneous frequency $f(t)$ is a single-valued function of time t, and there is only one definite frequency value at any moment. According to the degree of material damage, AE events with different frequency bands are defined in the frequency domain, and then, at a certain moment, we

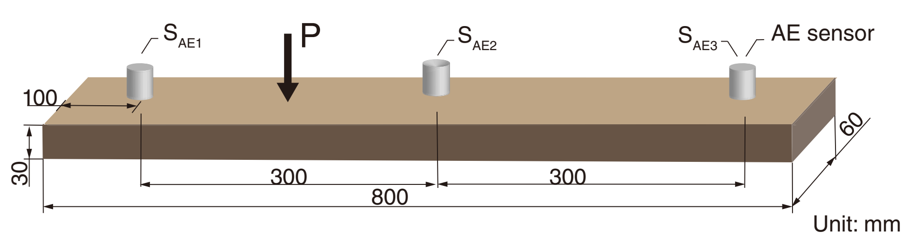

Figure 1.—Acoustic emission (AE) sensor layout diagram. P = applied external load.

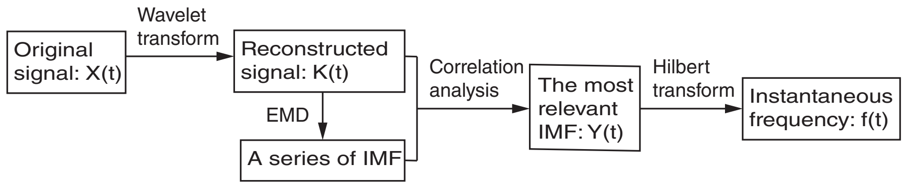

Figure 2.—Instantaneous frequency solving process.

only need to determine if the corresponding instantaneous frequency value falls within the range of that type of AE event. If so, the corresponding AE event is considered to have occurred.

Results and Discussion

Results and analysis of the three-point bending test

In the tests, we took the test data from ZS1 and PSM1 for analysis because of the large amount of AE signal data and the highly similar pattern of the damage process of specimens of the same tree species. The destruction process of wood under bending loads can be roughly divided into three typical stages: linear deformation stage, nonlinear deformation stage, and macroscopic fracture stage. The force–time variation curves of *Z. schneideriana* and *P. sylvestris* var. *mongolica* in the damage fracture process are shown in Figures 3a and 3b, respectively. The AE signal waveforms collected by the three sensors are basically similar during the bending damage process. So, only the signal waveform of sensor S_{AE2} was taken for analysis. The original AE signal waveforms corresponding to the two specimens are shown in Figure 4.

According to Figure 3a and Figure 4a, *Z. schneideriana* is in a linear deformation stage within 0 to 131 seconds, with elastic deformation occurring predominantly. The original AE waveform detected by the sensor also shows a high-amplitude AE phenomenon at the moment when there are several small fluctuations in the force–time curve, indicating that microcracking is occurring within the material at that stage. Within 131 to 208 seconds, the material is in the nonlinear deformation stage, *Z. schneideriana* begins to undergo significant plastic deformation, and the original AE signal waveform mainly shows many low-amplitude burst-type signals. At the same time, with the expansion of internal microcracks, some high-amplitude AE phenomena occur at this stage. At about 205 seconds, the load decreases significantly for the first time, which indicates that macroscopical damage of *Z. schneideriana* begins to appear at that time. At about 208 seconds, when the strength limit of the *Z. schneideriana* specimen is reached, the specimen starts to fracture macroscopically, while new microcracks appear inside the specimen and continue to nucleate and expand. Therefore, the AE signal waveform alternates between high-amplitude and low-amplitude burst signals.

According to Figures 3b and 4b, it can be seen that in comparison with *Z. schneideriana*, *P. sylvestris* var. *mongolica* undergoes a shorter linear deformation phase (0 to 40 seconds), which is characterized by the absence of any significant AE phenomenon in the early part of the phase, and then the material starts to undergo microcracking in the later part of the phase, which gradually results in the emergence of some AE signals with low-amplitude values. The original AE signals of the *P. sylvestris* var. *mongolica* specimen during the nonlinear deformation stage (40 to 340 seconds) are quite different from those of the *Z. schneideriana* specimen: In addition to low-amplitude signals, there are also many significant high-amplitude AE signals.

Compared to *Z. schneideriana*, *P. sylvestris* var. *mongolica* has longer fibers, which are affected by fiber bridging and have more pronounced nonlinear properties. According to the existing research (Lai et al. 2022), it is known that in the early stage of this phase, the difference between the tensile and compressive strengths of the wood leads to a shift in the neutral layer, which results in a small amount of AE. As the load continues to act, the shear gliding between the molecular chains of the stretched lignocellulose is intensified, and microfractures appear between the intercellular or cell-wall layers, resulting in a more intense AE phenomenon. Large numbers of fibers inside the material pull each other, while deformation and microscopic fractures occur, which leads to the phenomenon where large numbers of low-amplitude and high-amplitude AE signals coexist in the original AE waveform. At the macroscopic fracture stage (340 to 420 seconds), accompanied by the extension of a large number of microcracks and the formation of new cracks, significant brittle fracture occurred in the *P. sylvestris* var. *mongolica* specimen, and the AE signal characteristics were similar to those when macroscopic fracture occurred in the *Z. schneideriana* specimen.

From this analysis, it is obvious that it is not sufficient to identify material damage only by force–time curves or the original time-domain waveform of the AE signal. For example,

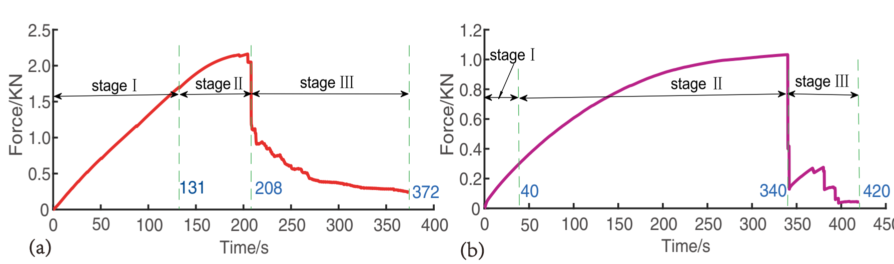

Figure 3.—Force–time curve of the three-point bending test. Stage 1: linear deformation stage; Stage 2: nonlinear deformation stage; Stage 3: macroscopic fracture stage. (a) Zelkova schneideriana *and (b)* Pinus sylvestris *var.* mongolica.

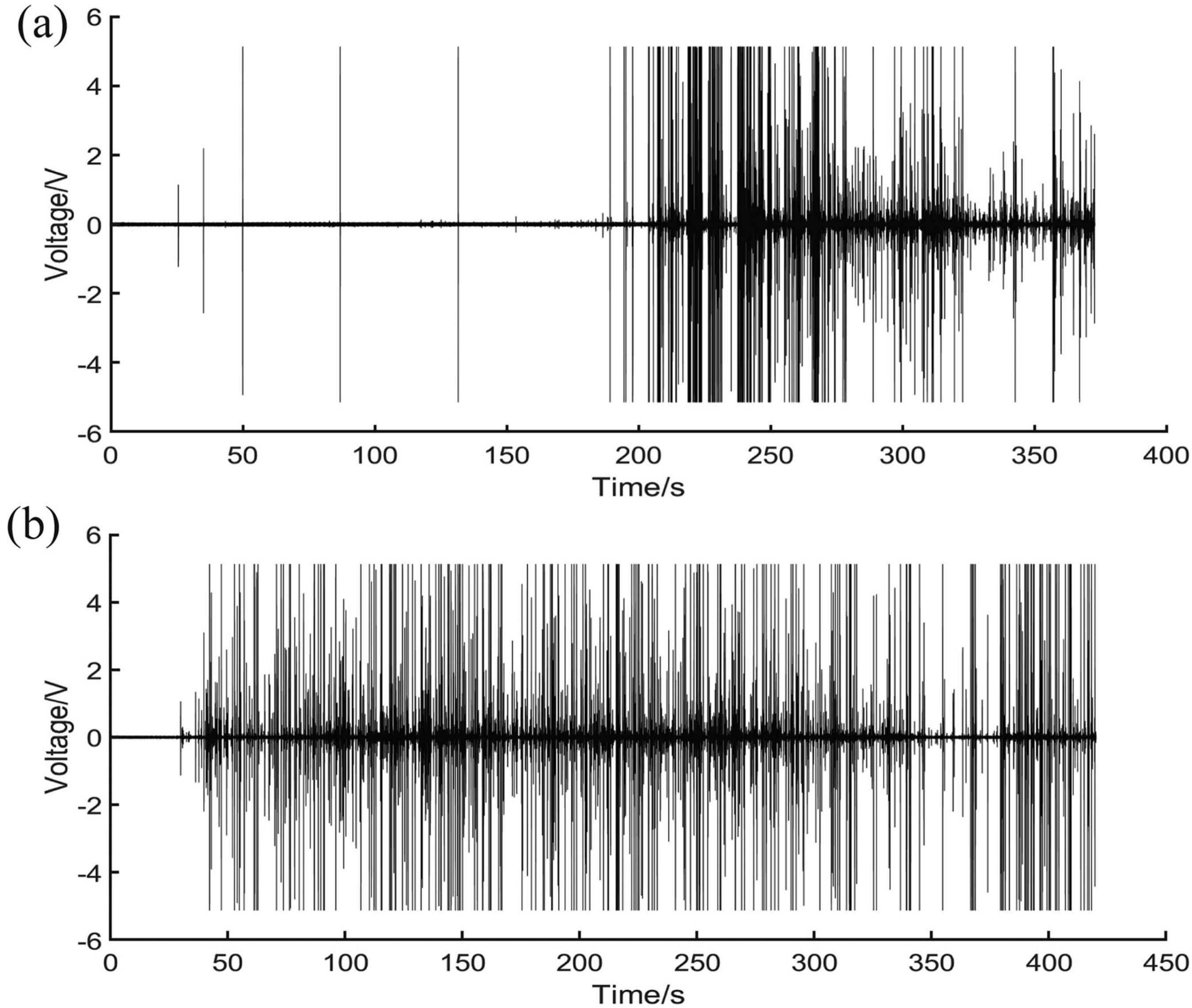

Figure 4.—Original acoustic emission (AE) signal waveforms. (a) Zelkova schneideriana. *(b)* Pinus sylvestris *var.* mongolica.

in the nonlinear deformation phase of the *P. sylvestris* var. *mongolica* specimen, damage has actually occurred within the wood, but the load curve has not fluctuated significantly. In addition, the time-domain waveforms of the AE signals of the *P. sylvestris* var. *mongolica* specimen show a very high similarity between the nonlinear deformation stage and the macroscopic fracture stage, but the actual damage conditions of the material differ significantly.

Frequency domain characteristics of AE signals at different damage stages

Due to the high sampling frequency, the data sets generated by the experiment were large, so we selected data with a length of 10^4 (20 ms) from three different damage stages of the specimens for discrete wavelet transform processing, and we reconstructed the AE signals on the basis of wavelet processing and then studied the frequency domain characteristics of the AE signals in different damage stages. The sensors S_{AE1} and S_{AE3} were close to the boundary of the specimens, and there were a large number of reflected waves in the original AE signals collected, which would affect the signal analysis. In addition, influenced by the viscoelastic property of wood, there would be a high-frequency attenuation of the AE signals in the propagation process (Wang et al. 2020); sensor S_{AE3} was farther away from the AE source, and the high-frequency attenuation phenomenon was significant, which had a greater impact on the analysis of signal characteristics. Therefore, in this article, the original signals acquired by sensor S_{AE2} were selected for analysis. The AE signal characteristics of the *Z. schneideriana* specimen and the *P. sylvestris* var. *mongolica* specimen at three different damage stages are shown in Figures 5 and 6, respectively.

In order to investigate the differences in the damage patterns of the two materials in the fracture process, the damage region of the specimen was individually selected to observe the damage on the compression and tension sides. Meanwhile, in order to further observe the internal damage of the material, the selected specimens were cut and their microscopic cracks were observed by XTL-100 electron microscope (Shanghai Yanfeng Precision Instrument Co., Ltd.; Figs. 7c and 7f). The details are shown in Figure 7.

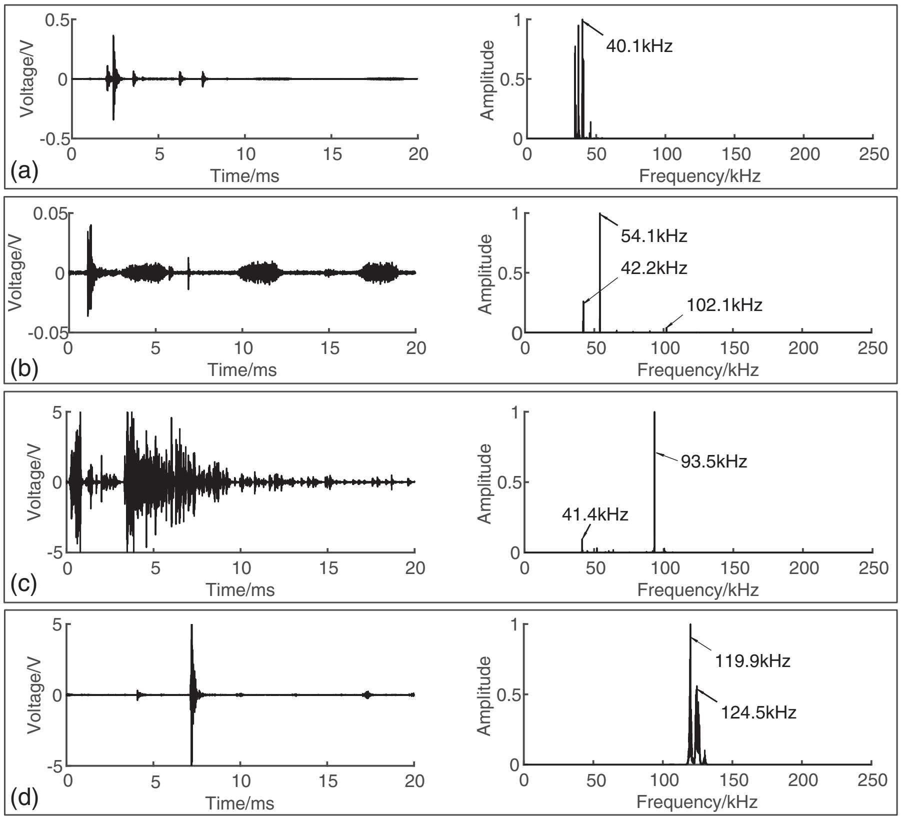

Figure 5.—The waveforms and spectrum of the reconstructed acoustic emission (AE) signal in Zelkova schneideriana *specimen at different damage stages: (a) linear deformation stage (25.679 to 25.699 seconds), (b) initial stage of nonlinear deformation (153.573 to 153.593 seconds), (c) later stage of nonlinear deformation (203.821 to 203.841 seconds), and (d) macroscopic fracture stage (211.416 to 211.436 seconds).*

According to Figure 5, in the linear deformation stage (Fig. 5a), the *Z. schneideriana* specimen is subjected to an external load, and the wood fibers in the compression zone are pressed into the interior of the specimen. However, due to the high flexural strength of *Z. schneideriana*, the squeezed wood fibers do not break significantly, but more linear deformation of the wood fibers occurs, and there is some extremely weak microscopic pulling. Upon continued loading, the wood cells in the compression zone are crushed and destroyed, and the surface of the specimen eventually forms the surface indentation shown in Figure 7b. The AE signals generated at this time are concentrated in the 30- to 45-kHz range, and the main frequency signal component is 40.1 kHz, which is a relatively low frequency signal component. In the early stage of the nonlinear deformation stage, the AE signal still mainly comes from the deformation of the material and the microscopic tensile fracture inside the material, and thus the AE signals are not only distributed in the low-frequency band centered at 42.2 kHz and 54.1 kHz, but also in the middle- and high-frequency band caused by the microscopic fracture (102.1 kHz). At the later stage of the nonlinear deformation stage (Fig. 5c), the microscopic cracks inside the specimen have been formed and gradually evolve to macroscopic cracks (Fig. 7c). At this time, microscopic ductile fractures replace material deformation as the main source of the AE phenomenon, and thus the AE signals are concentrated in the high-frequency band with 93.5 kHz as the center of distribution, while the signals in the low-frequency band are very few. During the macroscopic fracture stage (Fig. 5d), significant macroscopic ductile fracture of the *Z. schneideriana* specimen occurs under external loading, which eventually results in the formation of a pulling fracture wound as shown in Figure 7a. The AE signals produced are mainly characterized by high frequency and high energy, with a signal distribution frequency band of 117.6 to 132.8 kHz.

As shown in Figure 6, in the linear deformation stage (Fig. 6a), the AE signals collected from the *P. sylvestris* var. *mongolica* specimen are mainly distributed in the low-frequency band, as in the *Z. schneideriana* specimen, and the difference is that there are high-frequency signals centered at 102.1 kHz in the *P. sylvestris* var. *mongolica* specimen at this stage. This is mainly due to the fact that compared to *Z. schneideriana*, the *P. sylvestris* var. *mongolica* specimen is brittle and has many internal cavities, which means that the material bearing capacity is relatively low and sensitive to external loads. In the linear deformation stage, the wood fibers are pressed against each other by the load, resulting in deformation of the material, while some of the fibers that are pressed into the material by the extrusion of the surface fibers reach their strength limit, and microscopic brittle fracture occurs, resulting in the formation of a more obvious fracture phenomenon on the surface of the material, as shown in Figure 7e, thus producing both high-frequency and low-frequency signals. At the early stage of nonlinear deformation (Fig. 6b), as the degree of deformation intensifies, the microscopic brittle fracture of the *P. sylvestris* var. *mongolica* specimen becomes more and more obvious, and the proportion of high-frequency signal components increases, gradually replacing the low-frequency signal

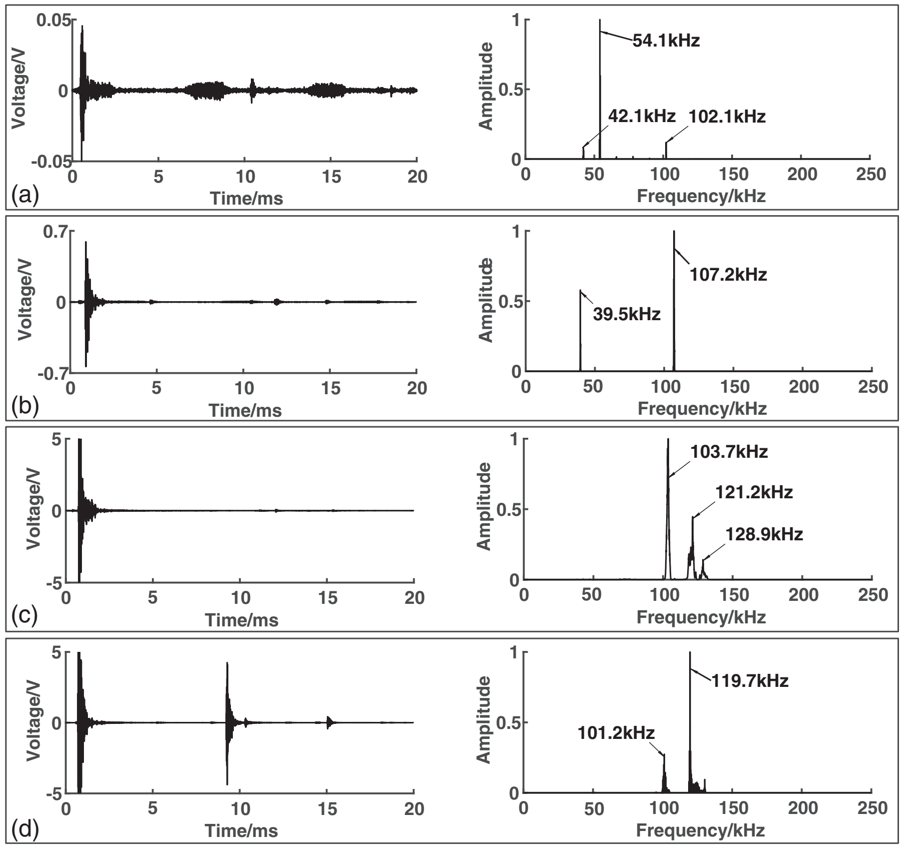

Figure 6.—The waveforms and spectrum of the reconstructed acoustic emission (AE) signal in Pinus sylvestris *var.* mongolica *specimen at different damage stages: (a) linear deformation stage (28.361 to 28.381 seconds), (b) initial stage of nonlinear deformation (41.907 to 41.927 seconds), (c) later stage of nonlinear deformation (308.390 to 308.410 seconds), and (d) macroscopic fracture stage (379.406 to 379.426 seconds).*

generated by deformation as the main signal component at this stage. At the later stage of nonlinear deformation (Fig. 6c), microscopic brittle fracture damage mainly occurs in the material, with the center of the main frequency signal distribution at 103.7 kHz. At the same time, some of the microscopic cracks that accumulated in the early stages (as shown in Fig. 7f) gradually become macroscopic cracks that are recognizable to the naked eye, so there are also a large number of high-frequency signals in the range of 120 to 130 kHz. After entering the macroscopic fracture stage (Fig. 6d), under the continuous action of the load, the cracks on the tensile side of the specimen gradually spread to the interior of the material, and a significant macroscopic brittle fracture occurs, and finally a brittle fracture-type wound is formed on the surface of the material, as shown in Figure 7d. At the same time, the internal microcracks (Fig. 7f) continue to expand, so there are two frequency distribution centers of AE signals, 101.2 kHz and 119.7 kHz, and the frequency band of 119 to 130 kHz is the main component of the AE signals.

According to this analysis, the AE signals generated during the damage process of the two specimens can be divided into three categories by the frequency domain characteristics: the deformation AE signals generated during the linear deformation stage, the microfracture AE signals generated during the nonlinear deformation stage, and the fracture AE signals generated during the macroscopic fracture stage. In this article, these three signals were defined as deformation AE (DAE), microfracture AE (MAE), and fracture AE (FAE), respectively.

Statistics of AE events

The previous analysis shows that the method of identifying damage in wood in the frequency domain is more effective and objective than that in the time domain. In this article, the frequency bands of DAE, MAE, and FAE events were defined as [30 kHz, 60 kHz], [90 kHz, 115 kHz], and [115 kHz, 135 kHz], respectively, according to Figures 5 and 6. In order to determine the instantaneous frequency of the AE signals at a certain time, the reconstructed AE signals were first decomposed by EMD after wavelet transform, and the Hilbert transform was used to obtain the instantaneous frequency. In order to objectively reflect the AE event level of the specimen during the damage process, the occurrence density of the three types of AE events was calculated at intervals of 50 ms according to the frequency range of the FAE, MAE, and DAE determined in advance. Figures 8 and 9 respectively show the density curves of the three types of AE events during the whole loading process for the *Z. schneideriana* and *P. sylvestris* var. *mongolica* specimens.

According to Figure 8, in the early stage of linear deformation and nonlinear deformation, the density of DAE and MAE events is stable at a high level of 160 times/ms and 150 times/ms, respectively, while the density of FAE events is much lower than that of DAE and MAE events, being roughly distributed at 60 times/ms. This suggests that the deformation of *Z. schneideriana* under loading is accompanied by a high level of strain energy release due

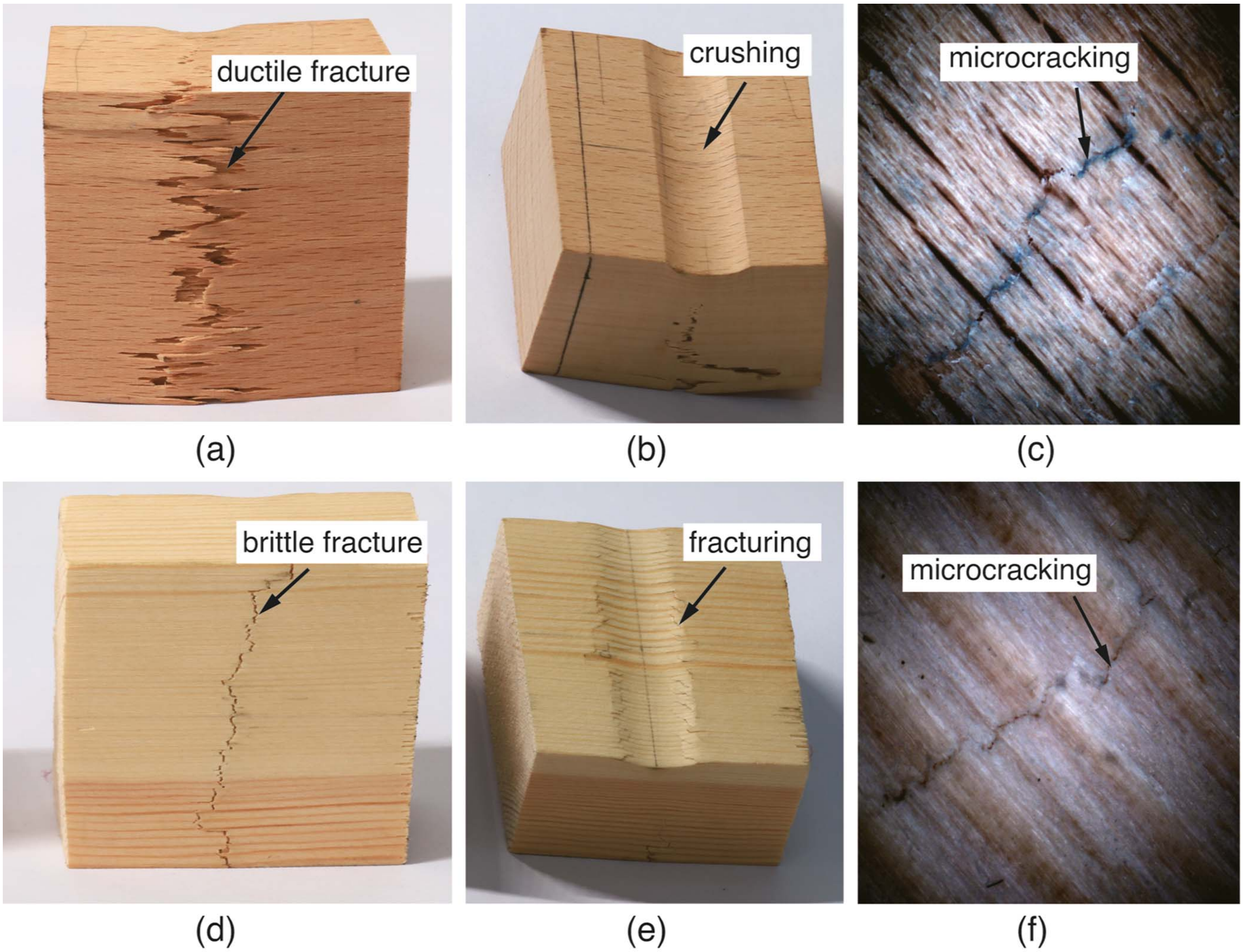

Figure 7.—Damage of specimens under load: (a) ductile fracture, (b) crushing damage, (c) microcracks in Zelkova schneideriana *specimen, (d) brittle fracture, (e) fracturing damage, and (f) microcracks in* Pinus sylvestris *var.* mongolica *specimen.*

to microtoughness fracture of the wood fibers as the fibers within the material pull against each other. However, the material still has a strong ability to resist damage, and the deformation and microscopic fractures that accumulate during loading are not sufficient to cause a macroscopic fracture recognizable to the naked eye. At the later stage of nonlinear deformation, the frequency of abrupt changes in the density of the three types of AE events shows a decreasing trend, which indicates that the material has yielded at this stage and has a strong ability to resist the external load, which coincides with the results that the load level rises at a slower rate in the range of 170 to 205 seconds in Figure 3a. At around 208 seconds, the density curve of DAE events undergoes a significant abrupt change, and the simultaneous abrupt change in the density levels of MAE and FAE events reaches a high value. This indicates that the cumulative deformation and microcrack extension (Fig. 7c) reach the maximum limit that the *Z. schneideriana* specimen can withstand, which leads to macroscopic fracture of the material, as shown in Figure 7a. There is also a large number of new microscopic cracks nucleating and expanding at this stage, as shown in Figure 7c, which is consistent with the result of Figure 3a, where the *Z. schneideriana* specimen loses its ability to resist the load and appears to fracture macroscopically at 208 seconds.

After that, as the load continues to act, the original microscopic cracks continue to expand, leading to further macroscopic fracture. Some internal areas of the material have not yet occurred damage, but with the continuous action of the external load, deformation accumulation gradually appears, thus generating new microscopic cracks, and the new cracks continue to expand, further aggravating the macroscopic fracture of the specimen. Therefore, the density curves of MAE events and FAE events remain synchronized to increase or decrease at a certain level, and where there is an abrupt change in the density of corresponding DAE events, there is a synchronized increase in the density of MAE events.

As shown in Figure 9, the density curves of the three types of AE events are maintained at a low level during the linear deformation stage of the *P. sylvestris* var. *mongolica* specimen, and there is almost no abrupt change in signal generation except around 20 seconds. By the early stage of nonlinear deformation, the DAE event density as a whole remains stable at the level of 60 times/ms, whereas the MAE and FAE event density curves are increasing, which is different from the changes in the three types of AE event

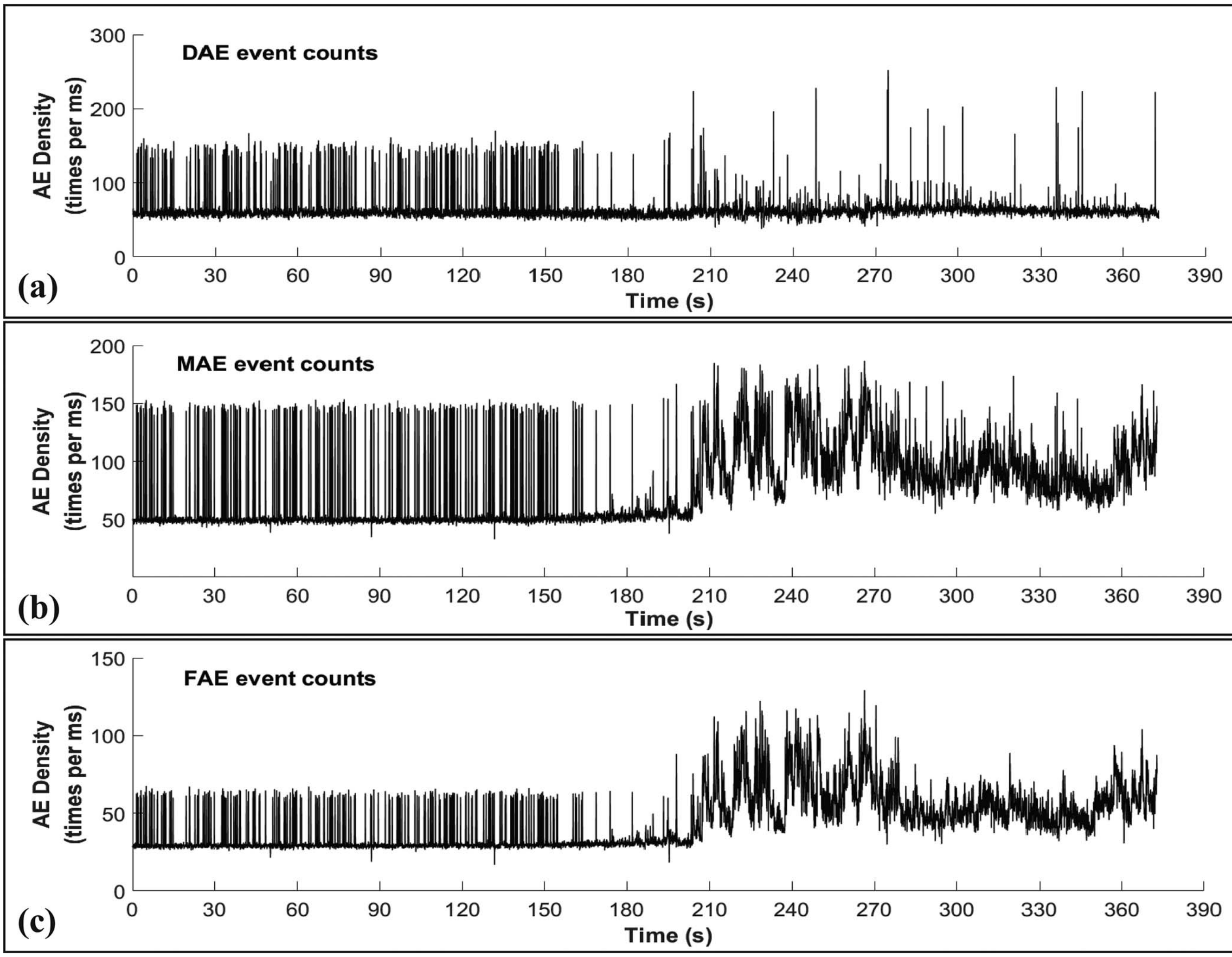

Figure 8.—Acoustic emission (AE) event density of the Zelkova schneideriana *specimen: (a) density statistics of deformation acoustic emission (DAE) events, (b) density statistics of microfracture acoustic emission (MAE) events, and (c) density statistics of fracture acoustic emission (FAE) events.*

density curves in the *Z. schneideriana* specimen. The main reason for this is that, compared to *Z. schneideriana*, the internal structure of *P. sylvestris* var. *mongolica* is more porous and brittle, which make it less resistant to loads. Therefore, a lower load level at the beginning of loading can trigger the fracture of the wood fibers on the surface of the material (as shown in Fig. 7e), which leads to microscopic brittle fracture (as shown in Fig. 7f) of the wood fibers near the loading point without the need for a long time of deformation accumulation.

At the late stage of nonlinear deformation, the crushed but unbroken wood fiber groups had a strong resistance to the load effect, which mainly caused the accumulation of plastic deformation. At the same time, the undamaged areas under the crushed layer were loaded to form a new crushed region, which led to the microscopic brittle fracture of a large number of wood fibers, so there were multiple abrupt changes in the density of DAE and MAE events.

Before the macroscopic fracture stage, with the continuous action of external loads, a large number of the ductile fibers without brittle fracture formed an extrusion effect on the adjacent xylem vessel, and the xylem vessel wall was forced to collapse into the internal cavity. The originally relatively dispersed fibers were gathered together to form a new bonding structure, and the energy exerted by the external load was constrained by the new bonding mechanism of the wood, which made the material less sensitive to the load, and therefore the specimen underwent a longer period of nonlinear deformation accumulation. Therefore, before the macroscopic fracture, the density of FAE events remained stable and was maintained at a certain level. The abrupt change of MAE and FAE event density at 340 seconds indicates that the material lost its ability to resist load damage and began to undergo macroscopic fracture, which is consistent with the sudden downward change in the stress level and macroscopic brittle fracture of the *P. sylvestris* var. *mongolica* specimen at 340 seconds in Figure 3b. After that point, the cracks within the material continued to develop, and the density curves of all three AE events show varying degrees of fluctuation.

Figures 8 and 9 show that defining and counting AE events in the frequency domain by instantaneous frequency not only can better distinguish different types of AE signals, but also the frequency of abrupt changes in the density can effectively characterize the damage of the material and the

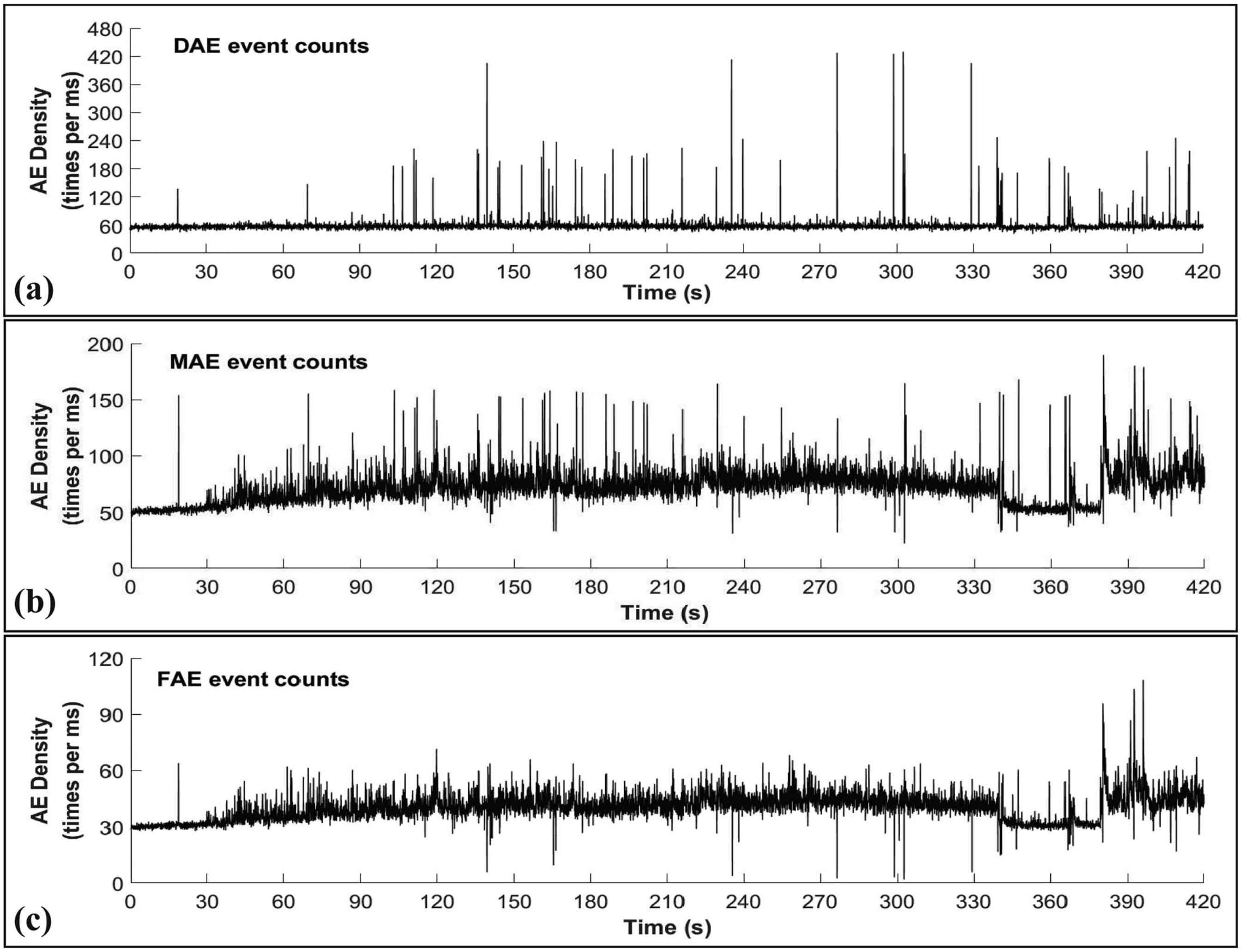

Figure 9.—Acoustic emission (AE) event density of the Pinus sylvestris *var.* mongolica *specimen: (a) density statistics of deformation acoustic emission (DAE) events, (b) density statistics of microfracture acoustic emission (MAE) events, and (c) density statistics of fracture acoustic emission (FAE) events.*

degree of intensity of the event, and even characterize the material properties to a certain extent. *Zelkova schneideriana* has high toughness and compact arrangement of internal wood fibers. Before the occurrence of macroscopic ductile fracture, the material properties showed that the levels of DAE, MAE, and FAE event densities were stabilized at a high level, and the three AE event densities had a high frequency of abrupt changes, which indicated that the damage to the *Z. schneideriana* specimen was characterized by a significant accumulation of strain with an extremely intense stress-release process. In the fracture stage, the frequency of abrupt changes in the density of DAE events was significantly reduced, while MAE and FAE events changed abruptly and significantly, indicating that the type of material damage in this stage was mainly high-strength microfracture and macroscopic ductile fracture.

Pinus sylvestris var. *mongolica* has a brittle texture and a more dispersed arrangement of wood fibers. At the beginning of loading, there was no obvious abrupt change in DAE event density, and there was a certain increase in MAE and FAE event density levels. The material properties were characterized by macroscopic fracture with higher intensity and extremely weak deformation accumulation. In the middle stage of loading, the dispersed fibers were gathered together, and the material showed strong resistance to damage. In the process of strain accumulation, the stress was released rapidly, so the DAE events showed obvious abrupt change with large amplitude, and the MAE and FAE events increased in the frequency of abrupt change, but the amplitude was small. Loading continued until macroscopic fracture occurred, and abrupt changes in the density of MAE and FAE events were evident, indicating that the stress release in the material became intense.

Conclusion

The parameter analysis method used in traditional AET usually sets AE thresholds in the time domain to identify AE events and then performs statistical analysis to characterize material damage. However, as a complex biomass composite material, wood has significant anisotropy, and it is very difficult to set the threshold of AE events. In this article, the AE signal characteristics of *Z. schneideriana* and *P. sylvestris* var. *mongolica* under bending load were studied based on the instantaneous frequency of the AE signals, and the damage of the wood was monitored based on the statistical analysis of the AE events. On the basis of the experimental study, this article summarizes the following conclusions.

There were three main types of AE signals produced by wood during the damage process: In the linear deformation stage, the wood fiber is pulled and squeezed to cause the material to deform and generate the DAE signal; the MAE signal is produced by microscopic fracture of wood fibers during the nonlinear deformation stage; and the macroscopic fracture stage, where microscopic crack growth in the wood fiber leads to macroscopic fracture of the wood, produces the FAE signal. The DAE signal is a low-frequency signal, the FAE signal is a high-frequency signal, and the MAE signal distribution frequency band is slightly lower than the FAE signal.

The AE event density curve can effectively characterize the stress state and damage of the material. The DAE event density curve can be used to describe the strain accumulation of a material. When the DAE event density is maintained at a high level, it means that the material has undergone linear deformation, and the material strain is intensified. The density curves of MAE and FAE events can be used to characterize the stress release and damage of the material. When the densities of MAE and FAE events are maintained at a high level, it implies that the fracture of the material is more significant, and the stress release is intensified. In addition, the frequency of abrupt changes in the density of AE events reflects the intensity with which the fracture phenomenon occurs, and the magnitude of its abrupt change reflects the strength of the material fracture.

There is a significant difference in the damage patterns exhibited by *Z. schneideriana* and *P. sylvestris* var. *mongolica* under loading, and this difference is mainly reflected in the density curve of the AE events; in other words, the density curve of the AE events characterizes the material properties to a certain extent. *Zelkova schneideriana* undergoes ductile fracture under load with a pulling wound on the tensile side of the specimen and a surface collapse on the compressed side. Prior to macroscopic fracture, DAE and MAE events show synchronous changes maintained at a high level; i.e., the material has a significant strain accumulation process prior to macroscopic fracture. At the beginning of a macroscopic fracture, the number of abrupt changes in DAE events decreases, and MAE and FAE events change sharply and abruptly upward and with a significantly higher number of abrupt changes. *Pinus sylvestris* var. *mongolica* undergoes brittle fracture under load, with flat crack wounds on the tensile side of the specimen and surface cracking on the compressive side. Before macroscopic fracture, the DAE events remained stable, the number of abrupt changes was less than that in the *Z. schneideriana* specimen, and the MAE event density curve fluctuated markedly, indicating that the material was less resistant to load, and microscopic fractures occurred in large numbers. When macroscopic fracture occurred, the density of MAE and FAE events changed sharply downward. Therefore, it is possible to distinguish between material properties and damage characteristics based on changes in the density curve of AE events.

Acknowledgment

This work was supported by the Excellent Young Research Project of Anhui Provincial Department of Education's University Research Program (No. 2022AH030160).

Literature Cited

Ando, K., Y. Hirashima, M. Sugihara, H. Sakiko, and S. Yasutoshi. 2006. Microscopic processes of shearing fracture of old wood, examined using the acoustic emission technique. *J. Wood Sci*. 52(6):483–489. https://doi.org/10.1007/s10086-005-0795-7

Chan, J. M., J. C. Walker, and C. A. Raymond. 2011. Effects of moisture content and temperature on acoustic velocity and dynamic MOE of radiata pine sapwood boards. *Wood Sci. Technol*. 45(4):609–626. https://doi.org/10.1007/s00226-010-0350-6

Chen, P., Q. M. Li, and T. Zhao. 2006a. Advances and trends in instantaneous frequency estimation methodology. *Elect. Meas. Instrum*. 43(7):1–7. https://doi.org/10.3969/j.issn.1001-1390.2006.07.001

Chen, Z., B. Gabbitas, and D. Hunt. 2006b. Monitoring the fracture of wood in torsion using acoustic emission. *J. Mater. Sci*. 41(12):3645–3655.

Choi, N. S., S. C. Woo, and K. Y. Rhee. 2007. Effects of fiber orientation on the acoustic emission and fracture characteristics of composite laminates. *J. Mater. Sci*. 42(4):1162–1168. https://doi.org/10.1007/s10853-006-1445-1

Ding, X. K., X. X. Zhang, Y. H. Hao, and J. Liu. 2012. Acoustic emission analysis during drying small thin wood samples. *China Wood Ind*. 26(3):40–43. https://doi.org/10.3969/j.issn.1001-8654.2012.03.011

Ding, X. Z., H. L. Zhao, K. N. Shen, and M. Li. 2015. Application of acoustic emission technique in wood drying. *J. Northwest Forestry Univ*. 30(3):242–244, 292. https://doi.org/10.3969/j.issn.1001-7461.2015.03.43

Dong, H. P. and M. Li. 2020. Wood acoustic emission event identification based on instantaneous frequency and damage monitor. *J. Northwest Forestry Univ*. 35(2):229–234. https://doi.org/10.3969/j.issn.1001-7461.2020.02.35

Fang, S. Y., R. Z. Qiu, and M. Li. 2018. Wood AE signal features based on improved EMD algorithm. *J. Vib. Shock* 37(23):292–298. https://doi.org/10.13465/j.cnki.jvs.2018.23.040

Gong, Y. X., M. C. He, Z. H. Wang, and Y. T. Yin. 2013. Research on time-frequency analysis algorithm and instantaneous frequency precursors for acoustic emission data from rock failure experiment. *Chin. J. Rock Mech. Eng*. 32(04):787–799.

Guo, Y., S. Zhu, Y. Chen, D. Liu, and D. G. Li. 2019. Acoustic emission-based study to characterize the crack initiation point of wood fiber/HDPE composites. *Polymers* 11(4):701–708. https://doi.org/10.3390/polym11040701

Huang, Z. H., C. F. Huang, J. W. Zhang, D. Z. Jiang, and S. Ju. 2018. Acoustic emission technique for damage detection and failure process determination of fiber-reinforced polymer composites: An application review. *Mater. Rev*. 32(7):1122–1128. https://doi.org/10.11896/j.issn1005-023X201807012

Jakieła, S., Ł. Bratasz, and R. Kozłowski. 2008. Acoustic emission for tracing fracture intensity in lime wood due to climatic variations. *Wood Sci. Technol*. 42:269–279. https://doi.org/10.1007/s00226-007-0156-3

Ju, S., M. Li, T. F. Luo, X. C. Li, M. H. Wang, X. S. Li, and J. Tu. 2020. Acoustic emission signal identification of wood damage process with instantaneous frequency. *J. Northeast Forestry Univ*. 48(2):87–92. https://doi.org/10.13759/j.cnki.dlxb.2020.02.016

Kang, H. and R. E. Booker. 2002. Variation of stress wave velocity with MC and temperature. *Wood Sci. Technol*. 36(1):41–54. https://doi.org/10.1007/s00226-001-0129-x

Kowalski, S. J., W. Moliński, and G. Musielak. 2004. The identification of fracture in dried wood based on theoretical modelling and acoustic emission. *Wood Sci. Technol*. 38:35–52. https://doi.org/10.1007/s00226-003-0211-7

Kowalski, S. J. and A. Smoczkiewicz. 2004. Acoustic emission in wood under drying. *Folia Forestalia Pol. Ser. B* 35:59–71.

Lai, F., M. H. Wang, S. Xiao, R. Ding, R. H. Luo, T. T. Deng, and M. Li. 2022. Detection of crack evolution characteristics of *Pinus sylvestris* var. *mongolica* using acoustic emission technology and image fractal theory. *J. Northeast Forestry Univ*. 50(7):89–93. https://doi.org/10.13759/j.cnki.dlxb.2022.07.011

Li, M., C. Huang, S. Fang, Y. Zhao, N. Xu, G. Qin, and F. Mao. 2023. Study on the effect of different angles on the propagation characteristics of acoustic emission signals in wood. *Sci. Prog*. 106(2):1–19. https://doi.org/10.1177/00368504231168532

Li, X. C., M. Li, and S. Ju. 2020. Frequency domain identification of acoustic emission events of wood fracture and variable moisture content. *Forest Prod. J*. 70(1):107–114. https://doi.org/10.13073/FPJ-D-19-00032

Mohammadi, R., M. Saeedifar, H. H. Toudeshky, M. A. Najafabadi, and M. Fotouhi. 2015. Prediction of delamination growth in carbon/epoxy composites using a novel acoustic emission-based approach. *J. Reinf. Plast. Comp*. 34(11):868–878.

Nasir, V., S. Ayanleye, S. Kazemirad, F. Sassani, and S. Adamopoulos. 2022. Acoustic emission monitoring of wood materials and timber structures: A critical review. *Constr. Build. Mater*. 350:128877. https://doi.org/10.1016/j.conbuildmat.2022.128877

Noguchi, M., S. Okumura, and S. Kawamoto. 1985. Characteristics of acoustic emissions during wood drying. *Mokuzai Gakkaishi* 31(3):171–175.

Rescalvo, F. J., M. Rodríguez, R. Bravo, C. Abarkane, and A. Gallego. 2020. Acoustic emission and numerical analysis of pine beams retrofitted with FRP and poplar wood. *Materials* 13(2):435–446.

Ritschel, F., Y. Zhou, A. J. Brunner, T. Fillbrandt, and P. Niemz. 2014. Acoustic emission analysis of industrial plywood materials exposed to destructive tensile load. *Wood Sci. Technol.* 48:611–631. https://doi.org/10.1007/s00226-014-0628-1

Sadanari, M. and S. Kitayama. 1989. Waveform analysis of acoustic emissions generated in the wood drying process. *Mokuzai Gakkaishi* 35(7):602–608.

Shao, Z. P., P. Chen, C. S. Zha, and K. Ji. 2009. Acoustic emission characteristics of damage and fracture process of wood and felicity effect. *Sci. Silvae Sin.* 45(2):86–91. https://doi.org/10.3321/j.issn:1001-7488.2009.02.016

Shen, K. N., H. L. Zhao, X. Z. Ding, and M. Li. 2015. Application of acoustic emission in wood processing. *World Forestry Res*. 28(1):56–60. https://doi.org/10.13348/j.cnki.sjlyyj.2015.01.008

Sun, J. P., F. H. Wang, X. D. Zhu, and L. Q. Yang. 2006a. Acoustic emission testing technology and its application prospect in non-destructive testing of wood materials. *World Forestry Res*. 19(2):55–60. https://doi.org/10.3969/j.issn.1001-4241.2006.02.011

Sun, J. P., F. H. Wang, X. D. Zhu, and L. Q. Yang. 2006b. Application of acoustic emission technology to damage process monitoring of wood under the dynamic loads. *J. Fujian Coll. Forestry* 26(4):58–62. https://doi.org/10.3969/j.issn.1001-389X.2006.04.013

Wang, M. H., T. T. Deng, S. Ju, X. C. Li, X. S. Li, and M. Li. 2020. Effect of wood surface crack on acoustic emission signal propagation characteristics. *J. Northeast Forestry Univ*. 48(10):19–25. https://doi.org/10.13759/j.cnki.dlxb.2020.10.015

Wu, Y., M. L. Pastor, M. Perrin, P. Casari, and X. J. Gong. 2023. Characterisation of damage mechanisms of GFRP-balsa sandwich under 4-point bending based on two-step clustering process in acoustic emission analysis. *Compos. B Eng*. 260:110774. https://doi.org/10.1016/j.compositesb.2023.110774

Yuan, P. P., Z. C. Wang, and W. X. Ren. 2016. Nonlinear model updating based on instantaneous frequencies and amplitudes of principal dynamic response components. *J. Vib. Eng*. 29(5):887–893. https://doi.org/10.16385/j.cnki.issn.1004-4523.2016.05.016

Zhao, Q., D. Zhao, and J. Zhao. 2020. Thermodynamic approach for the identification of instability in the wood using acoustic emission technology. *Forests* 11(5):534–560. https://doi.org/10.3390/f11050534

Zhao, R. J., X. B. Cheng, J. Sun, X. Q. Wang, and B. H. Fei. 2011. Study on the longitudinal tensile strength of the tracheids of soft wood. *J. Anhui Agric. Univ*. 38(4):491–495. https://doi.org/10.13610/j.cnki.1672-352x.2011.04.010